Rivista Italiana di Paleontologia e Stratigrafia
(*Research in Paleontology and Stratigraphy*)
vol. 126(2): 541-560. **July 2020**

CHRONOLOGY OF THE MESSINIAN EVENTS IN THE NORTHERNMOST PART OF THE MEDITERRANEAN: THE GOVONE SECTION (PIEDMONT BASIN, NW ITALY)

ROCCO GENNARI, FRANCESCA LOZAR, MARCELLO NATALICCHIO, ELENA ZANELLA, GIORGIO CARNEVALE & FRANCESCO DELA PIERRE

Dipartimento di Scienze della Terra, Università degli Studi di Torino, Via Valperga Caluso 35, 10125, Torino, Italy.
E-mails: rocco.gennari@unito.it; francesca.lozar@unito.it; marcello.natalicchio@unito.it; elena.zanella@unito.it; giorgio.carnevale@unito.it; francesco.delapierre@unito.it

To cite this article: Gennari R., Lozar F., Natalicchio M., Zanella E., Carnevale G. & Dela Pierre F. (2020) - Chronology of the Messinian Events in the northernmost part of the Mediterranean: the Govone section (Piedmont Basin, Nw Italy). *Riv. It. Paleontol. Strat.*, 126(2): 541-560.

Keywords: Messinian; biostratigraphy; magnetostratigraphy; Piedmont Basin.

Abstract. In marginal Mediterranean sub-basins the first phase of the Messinian salinity crisis (MSC) is recorded by primary sulfate evaporites (Primary Lower Gypsum unit); in deeper settings, the gypsum makes lateral transition into shales and marls usually barren of calcareous fossils that can hamper the identification of the MSC onset. The Govone section (Piedmont Basin, NW Italy) represents an opportunity to examine in detail the pre-MSC interval and the transition to the first stage of the MSC in a relatively deep marginal basin in the northernmost sector of the Mediterranean. We provide herein an age model for the Govone section, based on an integrated stratigraphic study, including cycloctratigraphy, magnetostratigraphy and micropaleontology (foraminifera and calcareous nannofossils) of the pre-MSC interval and the transition to the MSC. Chron C3An.1n has not been recognized in the study succession, most likely due to early diagenetic processes. Thus, the last occurrence of *Turborotalita multiloba* occurring two lithological cycles above the second influx of *G. scitula*, is the event that best approximate the MSC onset and is consistently recorded across the Piedmont Basin, with higher abundance respect to coeval Mediterranean successions. The calibration of the lithological cyclicity by means of these two bioevents allowed to recognize that, unlike other Mediterranean sections, the disappearance of calcareous microfossils occurs before the MSC onset, probably, in response of diagenetic processes favouring the dissolution of calcareous shells.

Introduction

In the Mediterranean region, open-sea middle and upper Miocene successions commonly display a precession-paced lithological ciclicity (Hilgen et al. 2003 and references therein). Approximating the base of the Messinian, the interval preceding the onset of the Messinian salinity crisis (pre-MSC, 7.16 – 5.97 Ma) records the progressive isolation of the Mediterranean Sea from the Atlantic Ocean produced during a long trend paleoceanographic evolution towards more restricted conditions (Kouwenhoven et al. 2003). These conditions enhanced the contrast of the sedimentary and biological response to high and low precession phases. The pre-MSC is well documented in a number of Mediterranean onshore successions from west to east, where the trend towards more restricted conditions is punctuated by four synchronous paleoceanographic steps (Hilgen & Krijgsman 1999; Sierro et al. 2001; Blanc-Valleron et al. 2002; Sierro et al. 2003; Kouwenhoven et al. 2006). This trend culminated with the widespread deposition of evaporites during the

Received: February 10, 2020; accepted: June 03, 2020

Messinian salinity crisis (MSC 5.97-5.33 Ma; Iaccarino et al. 1999; Manzi et al. 2013), a major geological event during which the Mediterranean was transformed into the youngest Salt Giant in Earth history (e.g., Hsü et al.1973; Roveri et al. 2014).

The four paleoceanographic steps punctuating the pre-MSC interval have been described as follows:

1) Starting at 7.16 Ma, the reduction of sea floor oxygenation (Kouwenhoven et al. 2006) is recorded by the disappearance of oxyphilic benthic foraminifera and by deposition of sapropelitic layers at every insolation maxima (precession minima) in deep-water successions (Krijgsman et al. 2004).

2) At 6.7 Ma, the deposition of sapropelitic layers started also at shallower depth (Sierro et al. 2001), even though locally discontinuous (Pissouri and Tokhni sections, Kouwenhoven et al. 2006; Gennari et al. 2018), indicating that low oxygen sea floor also reached intermediate depth during precession minima; during this step, the intermediate-dwellers globorotalids became less frequent and the *Globorotalia miotumida* gr. disappears from the Mediterranean (Sierro et al. 2001; Morigi et al. 2007); diatomaceous marls formed instead during precession maxima (Filippelli et al. 2003).

3) At 6.4 Ma benthic foraminifer species adapted to reduced oxygen content and high nutrient/organic matter fluxes to the sea floor increased in abundance (*Bulimina*, *Bolivina* and *Uvigerina*, mainly; Sierro et al. 2003; Kouwenhoven et al. 2006; Iaccarino et al. 2008; Gennari et al. 2018). At the same time, planktic foraminifera recorded relevant paleonvironmental changes in the water column with the appearance of the endemic Mediterranean species *Turborotalita multiloba* at 6.4 Ma, and the coiling change of the negloboquadrinids from sinistral to destral at 6.34 Ma (Sierro et al. 2001).

4) At 5.97 Ma, the onset of the MSC (Manzi et al. 2013) is commonly marked by the disappearance of >125 μm foraminifera and by distinctive peaks in abundance of calcareous nannofossil taxa (Manzi et al. 2007; Lozar et al. 2018; Manzi et al. 2018; Lozar & Negri 2019). However, while in the reference Falconara section the disappearance of calcareous microfossil marks the MSC onset (Hilgen & Krijgsman 1999; Blanc-Valleron et al. 2002; Manzi et al. 2013), in some Sicilian sections calcareous microfossils can disappear from the sedimentary record well before the onset of the MSC (Catalano et al. 2016), making questionable the use of this criterion alone for the identification of the MSC onset.

The four paleoceanographic steps mentioned above have been placed in a solid chronological framework obtained through the integration of biostratigraphic, cyclostratigraphic, magnetostratigraphic and radiometric data of the pre-MSC successions (e.g. Hilgen & Krijgsman 1999; Krijgsman et al. 1999; Blanc-Valleron et al. 2002; Krijgsman et al. 2004; Kouwenhoven et al. 2006; Di Stefano et al. 2010; Gennari et al. 2013 and Gennari et al. 2018; Manzi et al. 2018).

Such improvement was associated with significant advances in the physical stratigraphic correlations between onshore marginal and intermediate to deep water basins (e.g. Roveri & Manzi 2006; Roveri et al 2014). Accordingly, during the first stage of the MSC (5.97 – 5.60 Ma), the sulfate evaporites of the Primary Lower Gypsum unit were deposited in relatively shallow water settings, whereas an evaporite-free succession, barren of calcareous microfossil, accumulated in deeper settings (Manzi et al. 2007; Dela Pierre et al. 2011; Gennari et al 2013, 2018; Lozar et al. 2018; Manzi et al. 2018; Lozar & Negri 2019). The absence of gypsum and the scarcity (Gennari et al. 2018) or absence (Catalano et al. 2016) of calcareous microfossils make the identification of the onset of the MSC in these deep water successions problematic. Although in deep water successions body fossils can be scarce or even absent, molecular fossils are usually well preserved (Sinninghe Damstè et al. 1995; Kenig et al. 1995; Manzi et al. 2007; Natalicchio et al. 2017; 2019; Sabino et al. 2020) and may provide fundamental information about the paleonvironmental and paleoceanographic evolution of the Mediterranean basin across the onset of the MSC. In this light, the Govone section (Piedmont Basin, NW Italy) was the object of a recent paleonviromental reconstruction based on the analysis of molecular fossils (Sabino et al. 2020) as it represents a unique opportunity to examine in detail the pre-MSC interval and the transition to the first stage of the MSC in a relatively deep water marginal basin in the northernmost sector of the Mediterranean. In this paper, by presenting detailed cyclostratigraphic, magnetostratigraphic and biostratigraphic (foraminifera and calcareous nannofossils) data we discuss the age model of the Govone section as proposed in Sabino et al. (2020).

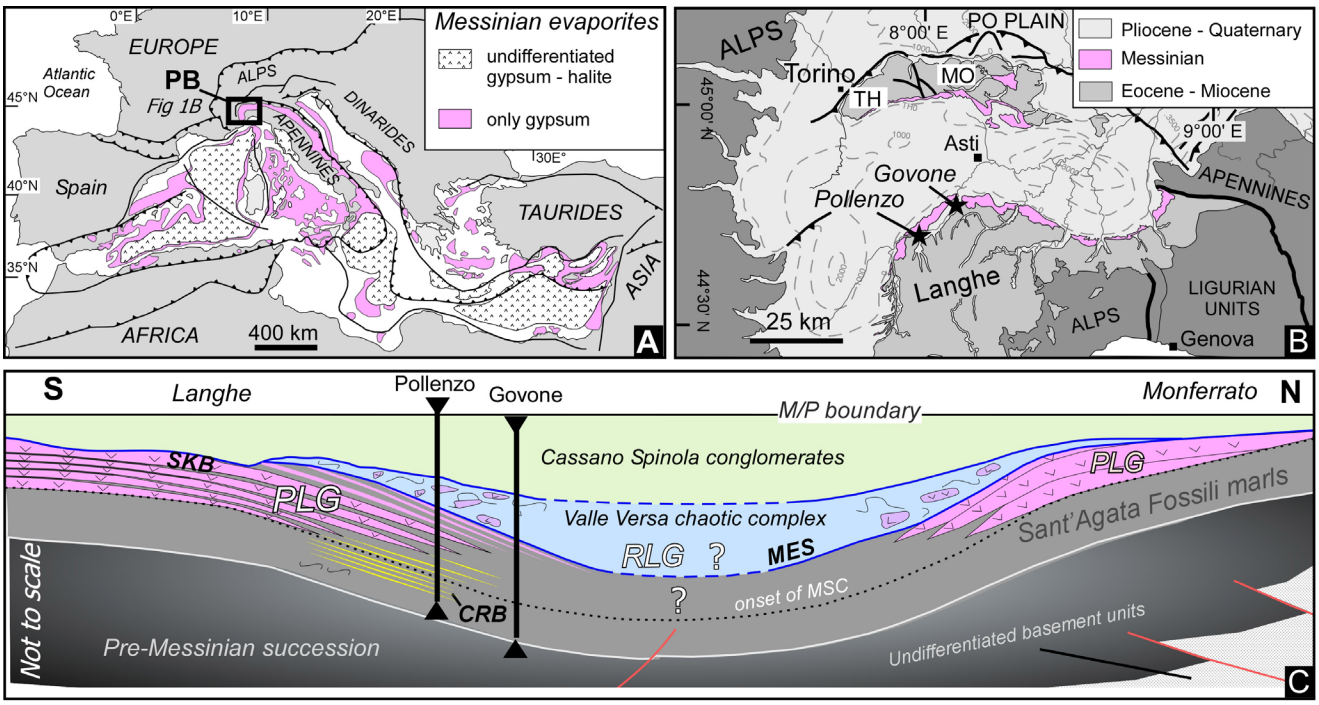

Fig. 1 - A) Distribution of the Messinian evaporites in the Mediterranean basin (modified from Manzi et al. 2013). PB: Piedmont Basin; B) schematic geological map of the Piedmont Basin and location of the Govone and Pollenzo sections (modified from Bigi et al., 1990. TH: Torino Hill; MO: Monferrato. C) Stratigraphic relationships between the Messinian deposits of the Piedmont Basin along a N-S profile, with location of the Pollenzo and Govone sections (modified from Dela Pierre et al. 2011). PLG: Primary Lower Gypsum; RLG: Resedimented Lower Gypsum; SKB: Sturani key-bed; CRB: carbonate rich-layers; MES: Messinian erosional surface.

Geological and stratigraphical setting

The Piedmont Basin (PB) is a wide wedge-top basin (Figs. 1A and B) filled with Eocene - Messinian sediments deposited upon Alpine, Ligurian and Adria units juxtaposed during the mesoalpine collisional event (e.g. Mosca et al. 2010; Rossi et al. 2009). Messinian strata are exposed in the northern and southern margins of the basin; in the depocenter they are buried below the Pliocene and Quaternary sediments of the Savigliano and Alessandria basins (Mosca et al. 2010; Rossi 2017).

The upper Miocene succession starts with outer shelf to slope fine-grained sediments referred to as the Sant'Agata Fossili Marls (Tortonian-lower Messinian) that record progressively more restricted conditions preluding the onset of the MSC (Sturani 1973; Sturani & Sampò 1973; Violanti et al. 2013). At the basin margins (Fig. 1C), this unit is followed by primary sulfate evaporites of the Primary Lower Gypsum unit (PLG), deposited during the first stage of the MSC (5.97-5.60 Ma, Dela Pierre et al. 2011). Both these units show a cyclic stacking pattern evidenced by the alternation of shales with bioturbated marls in the Sant'Agata Fossili Marls and with gypsum (both bottom grown selenite and cumulate gypsum) in the PLG unit. Carbonate layers of microbial origin are intercalated with the marls in the uppermost part of the Sant'Agata Fossili Marls in the Pollenzo section (Dela Pierre et al. 2012) as well as in the shales of the PLG unit (Dela Pierre et al. 2014). Micropaleontological (Lozar et al. 2010, 2018; Violanti et al. 2013) and geochemical (Natalicchio et al. 2017, 2019; Sabino et al. 2020) studies of the pre-MSC sediments (Sant'Agata Fossili Marls) indicates that the lithological cyclicity reflects precessionally-driven climate change, as in other Mediterranean basins (Hilgen et al. 1999; Blanc-Valleron et al. 2002; Sierro et al. 2001, 2003; Kouwenhoven et al. 2006; Manzi et al. 2007; Gennari et al. 2018). The same forcing mechanism is assumed to have driven the lithological cyclicity in the PLG unit (Vai 1997; Krijgsman et al. 1999). Towards the basin depocenter (Pollenzo and Govone sections, Fig. 1C) the PLG unit makes transition to a cyclical succession of shales and marls analogous to the pre-MSC conterparts and attributed, from a lithostratigraphic point of view, to the Sant'Agata Fossili Marls. In the Pollenzo section, where the up-

per part of the Sant'Agata Fossili Marls is exposed above a slumped interval, the onset of the MSC has been identified three precessional cycles below the lower gypsum bed (Dela Pierre et al. 2011; Lozar et al. 2018).

The PLG unit and its deeper water equivalent deposits are unconformably overlain by chaotic and clastic gypsum facies (Valle Versa Chaotic complex; Irace et al. 2005; Dela Pierre et al. 2007), which are correlated to the Resedimented Lower Gypsum unit deposited above the Messinian erosional surface (MES) during the second stage of the MSC (5.60-5.55 Ma; Roveri et al. 2014). The Messinian succession is closed by fluvio-deltaic and lacustrine sediments, referred to as the Cassano Spinola conglomerates (Ghibaudo et al. 1985; Dela Pierre et al. 2011, 2016; Fig. 1c), recording the third stage of the MSC (5.55-5.33 Ma; Roveri et al. 2008; Roveri et al. 2014).

Materials and Methods

The Govone section

The Govone section (44°48'08"N; 8°07'34"E) is located along the Tanaro River on the southern margin of the PB (Fig. 1). It represents the more distal section exposed in the PB and comprises the entire MSC record (Dela Pierre et al. 2011) (Fig. 2). The section starts with the Sant'Agata Fossili Marls that comprise 35 lithological cycles (the object of this study), made up of brownish laminated shales that are overlain by light grey massive marls (Figs. 3A, B and C). The shales commonly contain fish scales and isolated bones and plant debris; the marls are bioturbated and, especially in the lower part of the section, contain abundant bivalves, fish and echinoid remains. The cycles range in thickness from less than 1 m up to 2 m, and their stacking pattern is organized as an alternation or cluster of thinner (0-15 m interval) and thicker (15-20 m interval) cycles (Fig. 2). Evidence of sin-sedimentary instability was recognized at 27 m from the base of the section where a shear plane interpreted as a slump scar is present (Fig. 3D). In addition, in the topmost part of the unit, the presence of slumps makes the identification of the lithological cyclcity difficult. However, the shale/marl couplets are still recognizable, allowing to exclude any doubling of the succession and to identify three additional lithological cycles (Gm 33, Gm34 and Gm 35) below the lower gypsum-bearing cycles of the PLG unit.

The Sant'Agata Fossili Marls are followed by the PLG unit which is composed of nine lithological cycles represented by shale/gypsum couplets. The gypsum beds, up to 1 m thick, are thinner than those found in the more marginal sectors of the Piedmont Basin (i.e. Pollenzo). They consist of laminated gypsiferous silty mudstones with tiny randomly oriented crystals of primary gypsum, floating within an abundant clayey fraction; isolated flat conical structures, composed of clusters of mm to cm-sized selenite crystals and referred to the branching selenite facies (Lugli et al. 2010), are also common (Fig. 3E). Above the PLG unit, clastic gypsum facies, composed of normally graded beds of gypsrudites and gypsarenites are observed. They are interbedded with slumped laminated mudstones and with chaotic intervals. These resedimented facies are attributed to the Valle Versa Chaotic complex (Irace et al. 2005; Dela Pierre et al. 2007) that is considered equivalent to the Resedimented Lower Gypsum unit (RLG) deposited during the second stage of the MSC (5.60-5.55 Ma; Roveri et al. 2014). In the Govone Section this unit is floored by a sharp surface corresponding to the MES (Fig. 3F). The resedimented facies are finally overlain by fluvial to deltaic terrigenous deposits composed of conglomeratic beds (Cassano Spinola Conglomerates) deposited during the third stage of the MSC (Dela Pierre et al. 2011), i.e. from 5.55 to 5.33 Ma (Roveri et al. 2014).

Magnetostratigraphy

Fourty-five oriented standard paleomagnetic samples were collected using an electric drill. Specimens were thermally demagnetized by increasing steps of 20-30 °C up to a maximum of 410 to 540 °C and the natural remanent magnetization (NRM) was measured with a 2G ENTERPRISES DC-SQUID cryogenic magnetometer at the ALP Laboratory (Peveragno, Italy). Magnetic susceptibility was monitored to check changes in magnetic mineralogy throughout the heating process.

The NRM intensities vary from 0.003 to 0.081 mA/m with an average value of 0.02 mA/m. In the 75% of the specimens, at 380 °C, magnetization intensities are still at 30% of their initial value. Heating at 410 °C resulted in an increase in both the remanent intensity and the magnetic susceptibility, suggesting the occurrence of mineral alteration during

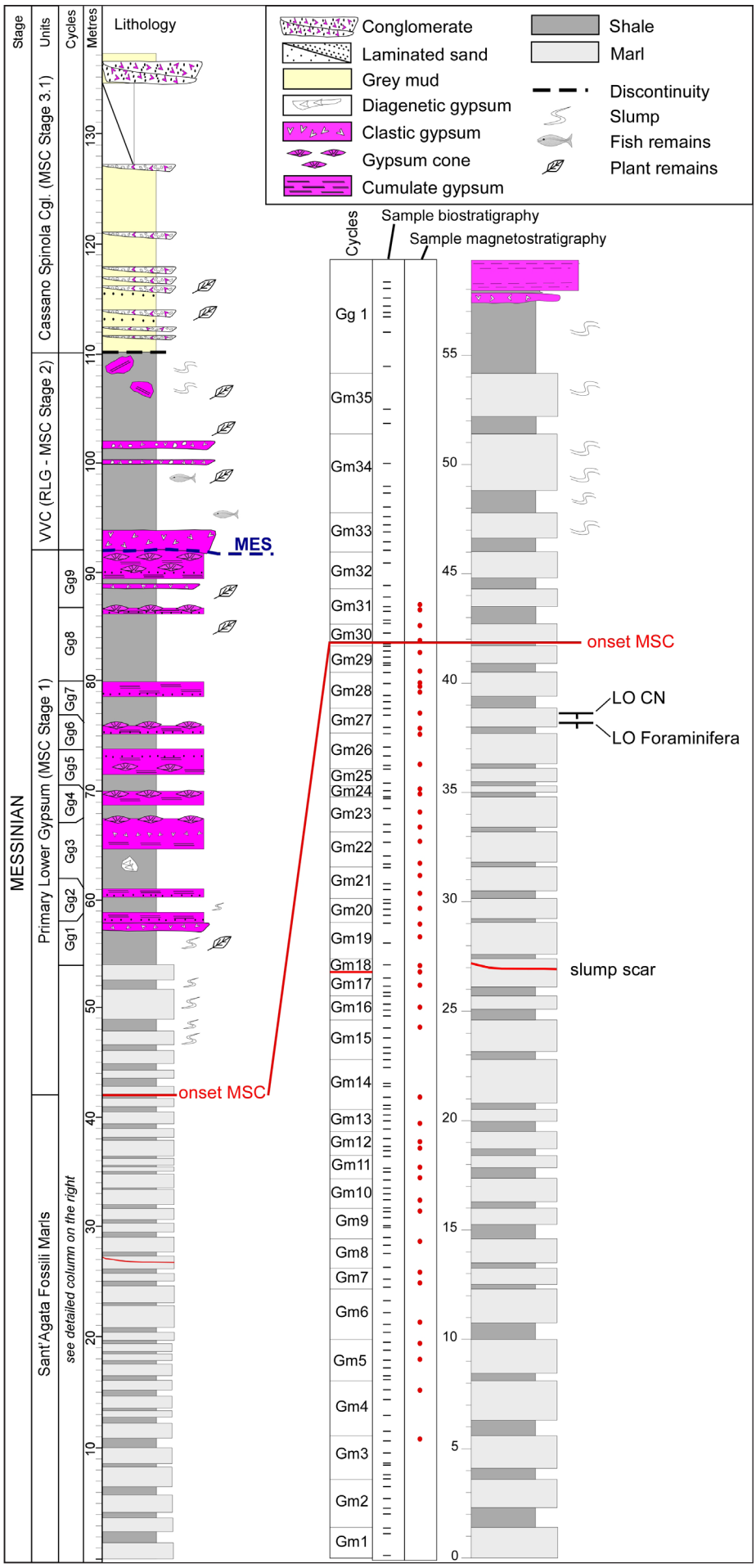

Fig. 2 - The Govone section (left) and detail of the studied part (right), with location of the studied samples and of the lithological cycles discussed in the text. MSC: Messinian salinity crisis; VVC: Valle Versa Chaotic complex; RLG: Resedimented Lower Gypsum unit; MES: Messinian erosional surface; LO: Last occurrence; Cn: calcareous nannofossils; F: foraminifera. Modified from Dela Pierre et al. 2016.

Fig. 3 - Field images of the Govone section: A) Lithological cycles in the Sant'Agata Fossili Marls (outlined by white dotted lines), consisting of laminated shale (sh)/marls (ma) couplets. B) The topmost part of cycle Gm25, composed of marls (ma) and the basal part of cycle Gm26, composed of laminated shales (sh). C) Stratigraphic level corresponding to the onset of the MSC (red line) in cycle Gm30. D) The shear plane (red line) separating cycles Gm17 and Gm18. (E) Detail of the PLG unit showing a flattened cone of gypsum growing within gypsiferous silty mudstones. (F). The Messinian erosional surface (MES) separating the PLG unit (below) from the Valle Versa Chaotic complex corresponding to the Resedimented Lower Gypsum unit (above). This latter unit is floored by a layer of gypsrudites (see inset), where some clasts are composed of twinned selenite crystals.

heating. After correction for bedding and core sample orientations, the mean characteristic remanent magnetization (ChRM) was calculated by principal component analyses of Zijderveld diagrams (Figs. 4A and B) by using the Remasoft software (Chadima & Hrouda 2006).

Micropaleontology

A total of 110 samples were collected to investigate the foraminifer assemblages; for every sample about 150 g of dry sediment were treated with hydrogen peroxide for 12 hours, boiled with water for about one hour, gently washed, sieved into grain fractions greater than 125 μm and 63–125 μm and weighed. Quantitative analyses were carried out on the residue greater than 125 μm, which was split into aliquots containing approximatively 300 planktic foraminifer tests, which were subsequently classified at the species level. In the same aliquots benthic foraminifera were counted to calculate the planktic/benthic ratio as P/(P+B)*100 (P/B ratio) and the composition of their assemblages was qualitatively observed. Planktic foraminifer species were organized in groups. *N. acostaensis*, *N. atlantica* (only present in the lower part of the section) and rare *N. humerosa* were lumped into the *Neogloboquadrina* gr. and were plotted as left and right coiled specimens, together with the right coiled ratio, calculated as (right specimens)/(right +left spcimens)*100. *Globigerinoides* gr. include *G. bulloideus*, *G. obliquus*, *G. extremus*, and minor *T. trilobatus* and *G. bollii*; the *Globoturborotalita* gr. is formed by *G. decoraperta*, *G. apertura*, *G. nephentes* and *G. woodi*. The *Globigerinita* gr. includes *G. uvula* and *G. glutinata*.

For calcareous nannofossils a subset of 81 samples was prepared and investigated. We used standard techniques for smear slide preparation in order to retain the original composition of the sediments (Bown & Young 1988) and performed cross-polarized light microscope observations at 1250 magnification. Qualitative observations werecarried out on the samples to check for biostratigraphic markers as well as to examine the trends associated to the lithological cyclic pattern. In Tab. 1, we report the preservation of the specimens (G = good, no etching or overgrowth; M = moderate, slight etching or overgrowth, P = poor, moderately etching or overgrowth), and their relative abundance estimates (very abundant, VA = more than 5 specimens/field of view (FOV); abundant, A = 2-4 specimens/FOV; common, C = one specimens/FOV; few, F = one specimens/ 5 FOV; rare, R = one specimens/ 10 FOV). We followed the taxonomy as presented in Perch Nielsen (1985), Young (1998) and Young et al. (2020). We lumped several species in groups as follow: *D. variabilis*, *D. surculus, D. pansus,* and *D. decorus* in the *Discoaster variabilis* gr.; *D. broweri, D. braarudi, D. asymmetricus,*and *D. calcaris* in the *D. broweri* gr. *Pontosphaera* spp. includes *P. multipora, P. discopora, P. japonica,* and *P. syracusana*; *Rhabdosphaera* spp. includes *R. procera* and *R. clavigera*.

Results

Magnetostratigraphy

The study of the Zijderveld diagrams (Figs. 4A and B) is limited to the temperature range of 20-380 °C since the heating at 410 °C causes a sudden rise in the magnetization intensity and the consequent random directions of the magnetization vectors of the values up 580 °C.

The specimens show both normal and reverse directions that are mostly well-defined, with a mean angular value (MAD) lower than 15.0°. All the specimens are affected by a normal viscous remanent magnetization (VRM), from 20 to 150 °C, consistent with the present magnetic field. In addition to the VRM, in the majority of the specimens (ca. 75%) of both polarities two remanent magnetization components are present, an intermediate temperature (Int-RM, 180-260 °C) component and a high temperature (High-RM, 290-380 °C) component. In the remaining specimens, only one remanent magnetization component is present in the 180-380 °C range (intermediate to high temperature, IH-RM, Fig. 4). The Zijderveld diagrams and the equiareal projections clearly show that each component is well-defined by the aligned values and no-overlapping trend is recognized (Figs. 4A and B).

Both the HighRM and the IH-RMcomponents point to the origin of the Zijderveld diagram and are interpreted as the Characteristic Remanent Magnetization (ChRM); this is the component considered for the magnetic polarity ascription. The Int-RM components are well-defined and with the same polarity of the ChRM, except in two cases where the intermediate and High-RM components are reversed and normal, respectively (samples rf 06 and rf 01, Fig. 5). Overall, the two sets of directions are quite similar, although these are clearly distinguishable as two separated clusters.

The mean-directions obtained by Fisher's Statistics (1953) of each component are well-defined with a_{95} values lower than 13.7° (Fig. 4C). For both the polarities, the Int- and the high-RM components are not statistically distinguishable, because

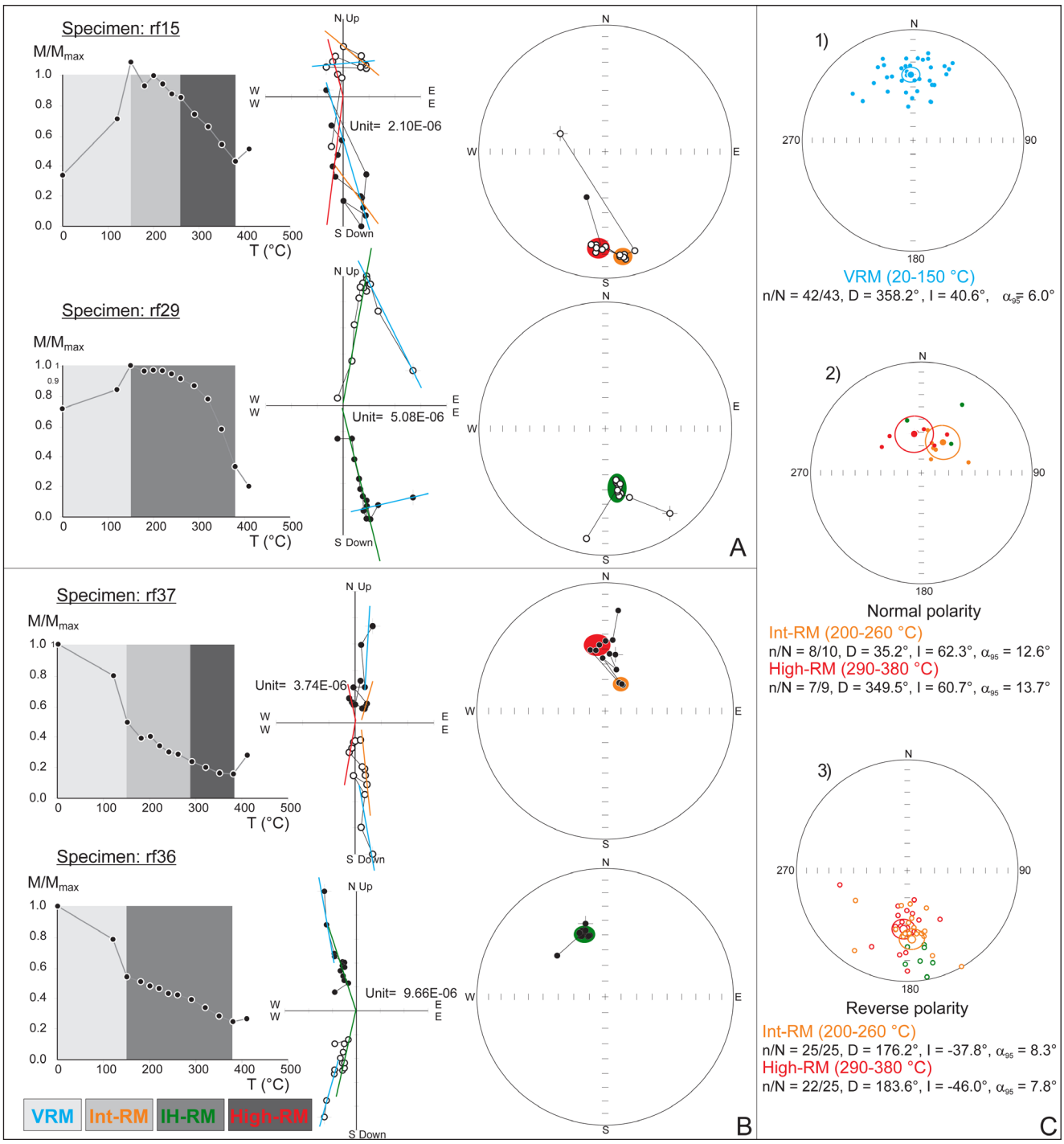

Fig. 4 - In A) and B) progressive thermal demagnetization results on reverse and normal polarity specimens, respectively. Left column: normalized intensity decay of the remanent magnetization. The grey boxes refer to the thermal range of each component (see below); middle column: Zijderveld diagrams. Solid/Open dots are the declination and apparent inclination values. The colored lines are the interpreted components: the VRM in light blue, the intermediate temperature component (Int-RM) in orange, the intermediate to high temperature (IH-RM) in green and the high temperature (High-RM) one in red; right column: equal-area projections of the magnetization directions. Solid/Open dot indicates positive/negative inclination. The colored area in orange, green and red refers to the above defined components. In C) equal-areal projections of the 1) VRM, 2) Normal polarity Int-RM, IH-RM and high-RM components, 3) Reverse polarity Int-RM, IH-RM and high-RM components. Symbols: solid/open dot = positive/negative inclination; large dot and ellipse = mean direction and 95% confidence limit, computed with Fisher's (1953) statistics. Colors as above.

their 95% confidence ellipses intersect. Moreover, the intermediate-T component is here interpreted as a secondary overprint that contributes to deflect the paleomagnetic direction by a few degrees, acquired within a short time delay after sediment deposition in an early diagenetic phase, and possibly attributed to the occurrence of iron sulphide phase, as greigite (Lucifora et al. 2012).

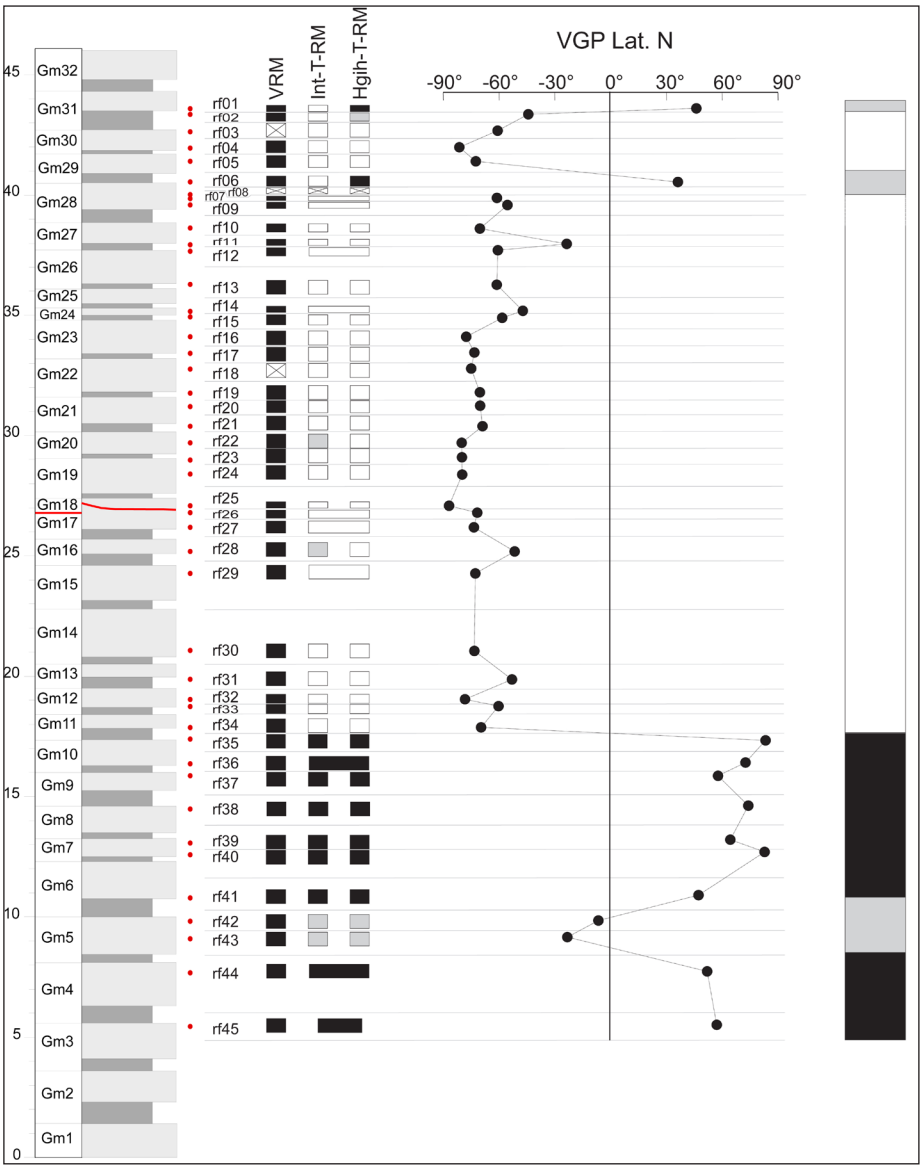

Fig. 5 - Magnetopolarity of the Govone section. From left to right: specimen name, polarity of VRM, Intermediate-T, high-T components (the crossed box stands for no-detection, the grey box indicates specimens with anomalous directions; larger boxes indicate evidence of one single magnetization component (IH-RM) instead of two (int-RM and high-RM), graph of the VGP Latitude as a function of the stratigraphic position, magnetic polarity (in grey, anomalous direction, undetermined polarity).

The Virtual Geomagnetic Pole was computed for each specimen and its latitude was plotted as a function of the stratigraphic position (Fig. 5), indicating two magnetopolarity zones: a normal magnetic interval in the lower part of the section from cycle Gm3 to Gm10 and a reverse polarity interval from cycle Gm11 upward. Only in four cases ambiguous directions were detected (Fig. 5). The meaning of such directions is unclear and further investigations are needed and will be addressed to a check and a better understanding of the mineralogy of the magnetization carriers in these layers.

Calcareous nannofossils

Qualitative observations show that calcareous nannofossils (CN) are abundant to common in the studied material, and are moderately to well preserved (Tab. 1), some barren levels occurs in cycles Gm19 (28.15 m), Gm20 (29.40 m) and Gm26 (36.65 m; Fig. 5 and Tab. 1). In particular, preservation is mostly good in the lower part of the section, up to 8.40 m (Gm5), then it becames moderate up to 22.5 m (Gm14); from this level, CN preservation shows a gradual deterioration trend from good to moderate, with poorly preserved assemblages observed from cycles Gm22 up to their las occurrence in cycle Gm27 at 38.50 m (event 19b, Fig. 6). In general, the assemblages are dominated by small placoliths, such as *Reticulofenestra minuta*, *Reticulofenestra haqi*, and *Umbilicosphaera jafari* and fairly abundant *Coccolithus pelagicus*, *Calcidiscus leptoporus*, *Pontosphaera* spp., *Helicosphaera carteri*, and *Rhabdosphaera* spp. Some of these taxa are alternatively dominant according to the lithotypes. *Discoaster* gr. (*D. variabilis* and *D. brouweri*) and *Sphenolithus abies* show higher abundances in the laminated shales; on the other hand, small placoliths

and *C. pelagicus* shows high relative abundances in the marls. The biostratigraphic markers *Reticulofenestra rotaria*, *Amaurolithus primus*, and *A. delicatus* are very rare but continuously present from the bottom of the section up cycle Gm27.

Foraminifera

As a general rule, foraminifera are more diversified and better preserved in the lower part of the section than in the middle/upper part. The absence of benthic foraminifera in laminated shales is regularly observed and identified by the peaks of the P/B ratio (up to 100%) (Fig. 6). The P/B ratio shows a cyclical pattern, generally showing lower values in the marly hemicycles, except for cycles Gm10 to 17, where the low number of benthic foraminifera lead to less pronounced P/B fluctuations. Both planktic and benthic foraminifera temporarily disappear in several layers, mostly in laminated shale (Gm6, Gm9, Gm21, Gm24 and Gm27), but also in the marls (Gm14, Gm23 and Gm26); consequently, these layers have no value in the P/B plot in Fig. 6. Absence of foraminifera is more frequent in the interval between 33 and 38 m (cycles Gm23-Gm27); above this interval foraminifera definitively disappear (event 19a at 38 m, Fig. 6).

Planktic foraminifera. The main components of the planktic foraminifer assemblages are *Orbulina universa*, *Globigerina bulloides*, *Neogloboquadrina* gr., *Turborotalita quinqueloba* and *Globigerinella pseudobesa*. *Globoturborotalita* gr., *Globigerinoides* gr., *Turborotalia multiloba*, globorotaliids (*G. miotumida* gr. and *G. scitula*), the *Globigerinita* gr. and *Globigerinella obesa* are less abundant or discontinuously present.

The dominant species exhibit wide relative abundance fluctuations, generally following the lithological cyclicity, with values ranging from 0 to 30-60% (Fig. 6). Warm-oligotrophic taxa (*O. universa*, *Globigerinoides* gr. and *Globoturborotalita* gr.; Sierro et al. 2003) have been plotted in the same graph (Fig. 6); among these taxa, *O. universa* is the dominant species and is particularly abundant in the laminated shale of cycles Gm6, Gm7 and Gm8 and from cycle Gm14 up to Gm27; noteworthy this taxon is absent in the marls with the exception for the cycle Gm21. *G. bulloides* preferentially occurs in the marls, but it can be consistently present (> 20%) also in some laminated shales; its relative abundance peaks exceed 20% from the base of the section up to cycle Gm18, where it becomes scattered and with relative abundance lower than 5%.

The *Neogloboquadrina* gr. shows higher abundances in the marls with respect to the shales up to the cycle Gm16, with the exception of a peak in the shale of cycle Gm2 (Fig. 6); in this lower interval, clusters of prominent abundance peaks (> 20%) are recorded in the cycles Gm4 to Gm6 and Gm14 to Gm16. From cycle Gm17 up to the disappearance of foraminifera in cycle Gm27, the *Neogloboquadrina* gr. shows no clear preference for any lithotype. As for the coiling direction, sinistral specimens prevail on dextral in the lower part of section up to cycle Gm14. From this level destral specimens gradually start to increase in abundance, showing high frequency fluctuations, with sinistral forms still abundant in several levels of the cycle Gm16, Gm17, Gm20, Gm21 and Gm26. Destral forms show prominent abundance peaks only from cycle Gm21 up to the complete disappearance of foraminifera in the cycle Gm27.

T. quinqueloba is almost exclusively present in the marls showing prominent abundance peaks (>40%) from cycle Gm18 upward (replacing *G. bulloides* within each lithological cycle; Fig. 6). *G. pseudobesa* is quite ubiquitous, being abundant in both marls and laminated shales, especially in the Gm7-Gm18 interval, thereby showing a long trend similar to that characteristic of *G. bulloides*. Below and above this interval both *G. bulloides* and *G. pseudobesa* become subordinated to either the *Neogloboquadrina* gr. and/or to *T. quinqueloba* in the marls, while *G. pseudoobesa* alone alternates with *O. universa* in the laminated shale. Other minor taxa are those of the *Globoturborotalita* gr. and *Globigerinoides* gr., which are generally associated with *O. universa* peaks. The *Globigerinita* gr. is ubiquitous from cycles Gm1 to Gm27 with low abundance (<5%) and shows a preference for marly hemicycles, where two prominent peaks occur (cycles Gm5 and Gm20). *T. multiloba* always occurs associated to the more abundant *T. quinqueloba*; the former species shows low abundances in the lower part of its range (<6%) and three prominent peaks in cycles Gm23, Gm25 and Gm26 (up to 40%).

Globorotaliids are rare to absent along the section, except in two levels. The *Globorotalia miotumida* gr. (represented by *Globorotalia miotumida* and *Globorotalia conomiozea*) is present from the base up to the cycle Gm8, being very rare (<1%) except in

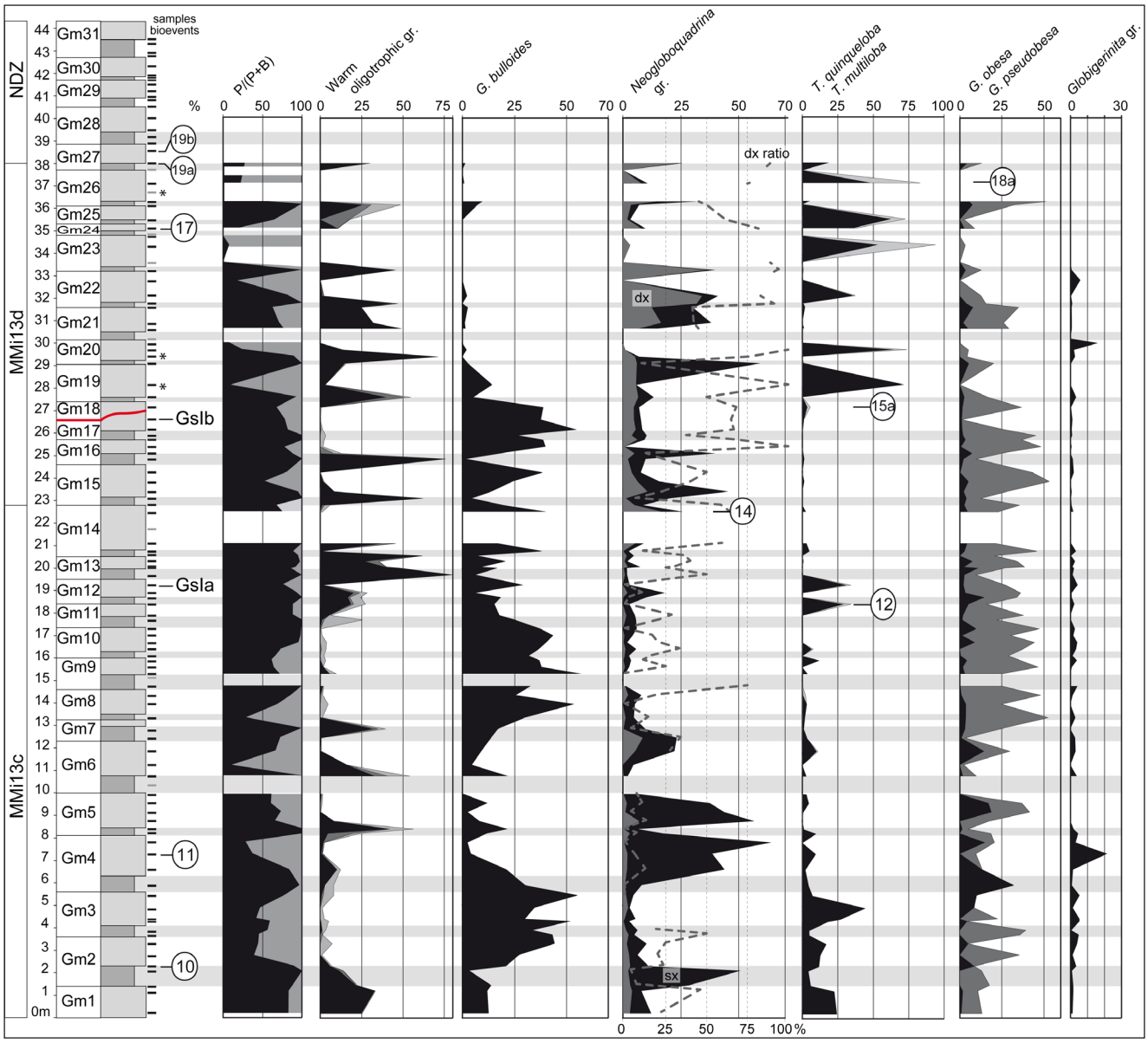

Fig. 6 - Plots of the P/B ratio and of the relative abundances of selected planktic foraminifer taxa. The warm and oligotrophic gr. (Sierro et al. 2003) is plotted as cumulative percentages of *Orbulina universa* (black), *Globigerinoides* and *Trilobatus* (dark grey) and the *Globoturborotalita* gr. (light grey). In the *Neogloboquadrina* gr. plot, dark grey is right coiled specimens, black is left coiled specimens and the dotted line is the ratio between right and left specimens. In the *T. quinqueloba/multiloba* plot, black is *T. quinqueloba* and light grey is *T. multiloba*. In the *Globigerinella obesa/pseudobesa* plot, black is *G. obesa* and dark grey is *G. pseudobesa*. Circles represent bioevents as labelled and described in the text: 10 is the last influx of *Globorotalia miotumida* gr.; 11 is the last regular occurrence of *G. miotumida* gr.; 12 is the first abundant occurrence of *T. multiloba*; 14 is the first abundant influx of the *Neogloboquadrina* gr.; 15a is the paracme end of *T. multiloba*; 17 is the second influx of *Globorotalia scitula*; 18a is the last occurrence of *T. multiloba*; 19a is the last occurrence of foraminifera and 19b is the last occurrence of calcareous nannofossil. GsIa and GsIb stand for the *G. scitula* minor influxes as reported in the text. In the left column the recognized biozones (Lirer et al. 2019) are reported. In the sample column, grey bars and asterisks represent levels where no foraminifers and no calcareous nannofossils occur, respectively.

the cycle Gm2 where it reaches 30%. *Globorotalia scitula* is continuously present but rare in the lowermost four cycles and then it occurs with two minor influxes in the cycles Gm12 and Gm17 (<1%) and a major one in the cycle Gm24 (18.4%).

Benthic foraminifera. As shown by the P/B ratio (Fig. 6), benthic foraminifera are generally dominant in the marly hemicycles. These cyclical increases in abundance are associated to changes in the assemblage composition allowing the recognition of three intervals from the bottom of the section to cycle Gm27. In the first interval, from cycles Gm1 to Gm10, the marly hemicycles (particularly in their central portion) are dominated by *Hanzawaia boueana*, *Melonis* spp. and *Cibicidoides* spp.

over the *Bulimina* gr. (mostly *Bulimina echinata* with rare *Bulimina aculeata*) and the *Bolivina* gr. (*Bolivina dentellata*, *Bolivina etrusca*, *Bolivina catanensis*, *Bolivina dilatata*, *Bolivina spathulata*). The second interval (Gm10-Gm18) is characterized by low abundance of benthic foraminifera so that the P/B ratio retains values higher than 60% also in the marls. This overall decreasing trend of abundance is associated with a frequency increase of the *Bulimina* and *Bolivina* grs. at the marl/shale transition or in the shales. From cycle Gm19 up to the complete foraminifer disappearance in cycle Gm27 (third interval), the P/B ratio shows again prominent peaks, with high fluctuations from 0 to 100%; benthic abundance peaks are here dominated by the *Bulimina* and *Bolivina* grs. only, while *H. boueana*, *Melonis* spp. and *Cibicidoides* spp. are completely absent.

Discussion

Cyclostratigraphy

The lithological cycles of the Govone section are mirrored by the cyclical pattern of the relative abundances of planktic foraminifer and, less regularly, benthic foraminifer assemblages. In addition, qualitative observations show that also calcareous nannofossils display similar fluctuations. Calcareous plankton taxa associated to warm and oligotrophic conditions such as *O. universa* among planktic foraminifera (Sierro et al. 2003) and *S. abies* and *Discoaster* spp. (Tab. 1) among calcareous nannofossils (Flores et al. 2005) are dominant in the laminated shales, where benthic foraminifera are particularly scarce or absent (Fig. 6). In contrast, in the marls planktic foraminifer assemblages representative of colder and more eutrophic environments are associated with a variable amount of benthic foraminifera, which either show a predominance of oxyphilic species (up to cycle Gm19) (Kouwenhoven et al. 2006) or of taxa adapted to low oxygen levels/high food availability (Kahio 1994). The calcareous nannofossil assemblages of the marly semicouplets are dominated by small placoliths (*R. minuta*, *R. haqi* and *U. jafari*) and *C. pelagicus* (Tab. 1), suggesting high nutrient levels, temperate climate, a well-mixed water column and a shallow nutricline (Flores et al. 2005).

The fluctuations between warmer/oligotrophic and colder/eutrophic calcareous plankton assemblages are commonly observed in the pre-MSC successions of the Mediterranean and are considered the response to climatic and oceanographic variations triggered by precessional forcing (Hilgen & Krijgsman 1999; Sierro et al. 2001; Blanc-Valleron et al. 2002; Kouwenohevn et al. 2006; Gennari et al. 2018; Lozar et al. 2018). During precession minima (insolation maxima), higher runoff (Simon et al. 2017) and warmer temperatures promoted an increased buoyancy of the surface waters and favored the stratification of the water column (Natalicchio et al. 2019). These conditions likely promoted the proliferation of warm water taxa in the uppermost water column and hindered the replacement of the oxygen consumed at the seafloor by the oxydation of the organic matter. The resulting bottom oxygen depletion prevented the proliferation of benthic foraminifera.

During precession maxima (insolation minima), the winter cooling promoted the mixing of the water column, the consequent fertilization of the surface layers and the oxygenation of the sea floor. This new configuration favored the proliferation of surface dwellers planktic foraminifera preferring cold temperature and high nutrients (*G. bulloides* and *T. quinqueloba*; Sierro et al. 2003), as well as the colonization of the seafloor by benthic foraminifera adapted to high nutrients levels, such as those of the *Bolivina* and *Bulimina* grs. (Murray 2006).

Biomagnetostratigraphic events

The Messinian age of the Govone section is suggested by the foraminifer *G. miotumida* gr. and the calcareous nannofossil *Amaurolithus delicatus* occurrences from its base. The first common occurrences (FCOs) of these taxa postdate the Tortonian/Messinian boundary at 7.24 Ma (Hilgen et al. 1995) and 7.221 Ma (Hilgen et al. 2000), respectively. Furthermore, the following planktic foraminifer bioevents (Fig. 6, labelled after Sierro et al. 2001 and modified in Gennari et al. 2018) were identified:

The last influx (LI, ca. 30%, event 10) and the last regular occurrence (LrO, event 11) of the *G. miotumida* gr. are observed in cycles Gm2 and Gm4, respectively. The former event was observed in the Perales section in the cycle UA7 dated at 6.55 Ma (Sierro et al. 2001). It predates the last (regular) occurrence of the *G. miotumida* gr., which is more commonly reported and dated at 6.50 Ma (see also Hilgen & Krijgsman 1999 and Kouwenoheven et al. 2006).

Tab. 1 - Qualitative estimates of calcareous nannofossil abundances in the Govone section. See text for the description of taxonomic group; preservation: G = good; M = moderate; P = poor; relative abundance estimates: very abundant, VA = more than 5 specimens/field of view (FOV); abundant, A = 2-4 specimens/FOV; common, C = one specimens/FOV; few, F = one specimens/ 5 FOV; rare, R = one specimens/ 10 FOV.

samples	meters	preservation	*C. pelagicus*	*Rhabdosphaera* spp.	*R. rotaria*	*R. pseudoumbilicus* gr.	*R. antarctica*	*R. minuta* (<3m)	*R. haqi* (3-5m)	*H. carteri*	*H. cf. sellii*	*S. abies*	*Cd. leptoporus* gr.	*Cd. macintyrei*	*Pontosphaera* spp.	*U. jafari*	*U. rotula*	*S. pulchra*	*B.bigelowii*	*C. murrayi*	*A. primus*	*A. delicatus*	*N. amplificus*	*D. variabilis gr*	*D. braweri* gr	*D. pentaradiatus*	*L. perdurum*
GOV A -2.1	0,20	G	C	F		P		F	F	C					C	A	P	R						P	P		
GOV A -2.2	1,20	M	F	C		P	R	A	C	F		P	C		F	R	R	F		P				P			
GOV A -1.1	1,45	G	C	C		P		R	F	F		P			C	A	P	R		R				R	P	P	
GOV A -1.2	2,10	M/G	R	R		P	R	VA	F	R	R	P	P		P	R	R	R		P				P		P	P
GOV A 1.1	2,30	M	R	R		P	R	VA	F	R	R	P	R		R	R	P	R						P		P	
GOV A -1.4	2,80	G	A	F	P	P		F	F	F	C	P	C		F	F	P	R	P					R	P	P	
GOV A 1.2	3,30	G	F	C				C	F	F	R	P	F		C	F	P	R		P				C	P	R	
GOV A 0.1	3,70	M	R	R		P	P	VA	C	F	P	R	F		R	R	P	R						R			
GOV A 0.2	3,90	M	R	F			P	VA	R	F	P	P	F		R	P	P	F						F		P	
GOV A 1.3	4,30	G	F	F	P	R		C	A	F		P	F		R	F	P	R		P				C	R	R	
GOV A 0.3	4,40	G	F	F		R		F	C	C		P	C		F	R	P	R						C	R	R	
GOV A 1.4	4,90	G	C	F	P	P		F	C	F	R	P	F		R	R	P	R						A	R	R	
GOV A 1.5	5,45	G	R	F	P			R	F	F	R	P	C		R	R		R		P				A	C	R	
GOV A 1.6	5,90	G	P	R	P			VA	R	P	P	P			R	F	P	R		P	P			P			
GOV A 2.1	6,60	G	F	F		R		F	C	F	F	R	R		R	P	P	R	A					P		P	
GOV A 2.2	7,30	G	F	R		R		VA	F	R	C	P			P	R		P						F			
GOV A 2.3	7,80	G	C	A		F		F	A	F	F	P			F			F	P	P				P			
GOV A 2.4	8,20	G	P	R				VA	F		P	R	P					P			P						
GOV A 2.5	8,40	G	P	F	P	P		VA	R	R	R	R	P		P	P	P	P		P				P		P	
GOV A 4.3	12,45	M	R			C		C	A	P	F				C				P					R			
GOV A 4.4	12,85	M		R	R	F		C	A	R		R	P		F						P	P		F			
GOV A 4.5	13,35	M	P		F	C		A	C	R	C		F		R	F						P					
GOV A 5.1	13,95	M	R	R	P	R		A	R	F	R	P	R	R	A	C		F			P		P	R			
GOV A 5.2	14,35	M	R	R		C		C	C	R		P	F	R	F	A					P	P		R		P	
GOV A 6.4	16,10	M	F	R		P		A	F	C	R	R	R		F	F	P		C					P			
GOV A 7.1	16,40	M	R	P		P		VA	P	R	R	P	P		F	A	P							P			
GOV A 7.2	16,70	M	C		P	P		A	F	A	R	R	F		F	R	R							P			
GOV A 7.3	17,00	M		P	P	P		VA	R	R	P		R		R	P	R			P				P			
GOV A 7.4	17,30	M	P	P		P		VA	P	R		P	R		R	P	P			P				R			
GOV A 7.5	17,70	M	P		P	P		VA	A	P		R	P		P	F	R										
GOV A 8.1	17,90	M	R			R		C	VA	F	R	P	R		P	R			P								
GOV A 8.2	18,40	M	C	P	P	R		C	VA	R	R	P	F		P	R	P		R					P			
GOV A 8.3	18,70	M	R		P	P		A	VA	P	R		P		P	P											
GOV A 9.1	18,90	M				R		VA	R	R	R	P	R			R											
GOV A 9.2	19,25	M	P	R		F	R	A	R	R	R		R		P	VA	P	R						P			
GOV A 9.3	19,70	G	P	P			P	A	A	R	P		P			A	R	P									
GOV A 10.1	20,00	M	F			R	R	A	F	P	P		P		P	A	R										
GOV A9.1bis new	20,15	M	F	P		R	P	A	R	R	R		R		P	A	R							P			
GOV A 10.2	20,30	M	F		P	R	R	VA	R	R	P	P	R			A	R							P			
GOV A9.2 new	20,55	G	R		P	P	P	VA	C	R	R		R			C	R							P			
GOV A 10.3	20,75	M	R	P		C	R	A	R	C	F	P	R		R	F	R	P						P			
GOV A 9.3 new	21,10	M	C		P	R	R	VA	R	R	P	P	P			C	R							P			
GOV A 9.4 new	21,75	M	C	P	P	P	R	A	P	F	R	P	P		P	A	P										
GOV A 9.5 new	22,50	M	F	R	P	C	P	C	R	F	R	P	A		P	A	R	R		P				P			P
GOV B 0.2	24,25	G		R		F		A	A	R			R		F						P		P	R			
GOV B 0.4	24,85	G			R	R		F	VA	F		R	F		R								P	F			
GOV B 1.1	25,10	G	P			F		A	F	C		P	F	R	F			P						P			
GOV B 1.2	25,40	G		R		A		A	C	C					F			R						P			
GOV B 1.3	25,70	G		R		R		A	VA	F					R			P			R		P				
GOV B 1.4	25,90	G		R	R	R		A	A	F		P	R		C			P				P		P			
GOV B 2.1	26,15	M/P	R	R		P	R	VA	F	F	R	P	P		F	F	F	R									
GOV B 2.2	26,60	G	P	R	P	R		A	A	R					F						P			P			
GOV B 2.3	27,15	G		R	P	A		R	F	C		P	C		C							P					
GOV B 2.4	28,15																										
GOV B 2.5	29,10	G	R		P	C		A	A	C		R	F	F	P							P					
GOV B 2.6	29,40																										
GOV B 3.1	29,70	G		C		R		C	R	A	C	P		P	C	C		R			P	P		P			
GOV B 3.2	30,00	G	R	C		R		R	R	A	A	P	P		F	C					R			P			
GOV B 3.3	30,20	G	R	C		R		A	R	F	R				C	C					R			C			
GOV B 4.1	30,65	M/G	P	P		P	P	VA	F	R	P		F		C		P	P						P			
GOV B 4.2	30,90	G	P	P			P	VA	C	R	R	P	R		F	P	R	P						P			
GOV B 4.3	31,60	G	P	R			P	VA	C	F	R		F		R	P	R	P						P			
GOV B 4.4	31,75	G	P	P			P	VA	A	R		F	P		R	P	P	P		P				P			
GOV B 4.1 BIS	32,10	M/P	R	P		R	R	A	F	C	F	F	R		F	P	P	R		P							
GOV B 4.2 BIS	32,80	VP	R	P		R	F	A	C	R	F	R	A		P	R	R	R									
GOV B 4.3 BIS	33,25	M/G	P	P		P	P	VA	A	F	P	R	P			P	R	P			R	P		P			
GOV B 5.1	33,60	P	R			P	R	F	F	R	P	P	VA				P									P	
GOV B 5.2	34,35	M	R	R	R	R	R	C	F	C	F	P	F		P	A	R	F						P			
GOV B 5.3	34,75	M	P	R		P	P	P	P	F	R		R		P	VA		R									
GOV B 5.4	34,81	M/G	R	P		C	R	A	A	P		P			P	R	P	P						P			
GOV B 6.1	35,10	M	R	R		F	P	A	F	A	P	P	R		F	R	P	R		P	R			P			P
GOV B 6.2	35,50	M/G	P	P		P		A	C	F		P	R		C	A	P	R			P			P			
GOV B 6.3	36,15	G	P	P		R	P	A	A	R		P			P		R	P						P	P		
GOV B 7.1	36,30	M/P	R	R			R		A	R	P	P	R		F	R	P	P						R			
GOV B 7.2	36,65																										
GOV B 7.3	37,10	M	P	R		P	P	VA	A	P			P		R	P		R		P							P
GOV B 7.4	37,70	G/M	P			P	R	VA	A	P			P				P					P		P			
GOV B 8.1	38,00	P	R	P		P	R	VA	F	R	P	P	P		P	P	P							P			

The first abundant occurrence (FAO, event 12) of *T. multiloba* is recorded in cycle Gm 12 (5.12%), immediately followed by a second influx in cycle Gm 13 (3.24%); the FAO was documented and dated by Sierro et al. (2001) in cycle UA15 of the Perales section at 6.415 Ma. These low occurrences are followed by a paracme which ends in cycle Gm 18 (PE, event 15a); from this cycle upwards other abundance peaks are recorded up to cycle Gm 26, where the last occurrence (LO, event 18a) of this taxon is observed. Although the relative abundances in the Govone section are considerably lower compared with other Mediterranean sections (e.g. Hilgen & Krijgsman 1999; Sierro et al. 2001), *T. multiloba* shows a remarkably similar pattern.

The remarkable abundance increase of destral neogloboquadrinids at the top of the thick cycle Gm14 confidently correlate the destral *N. acostaensis* FAO (event 14) of the Perales section (Sierro et al. 2001). However, above this event a straightforward and continuous dominance of destral forms is not observed in the Govone section; several fluctuations of the coiling ratio are still present in the Gm14-Gm27 interval and sinistral influxes, such as those observed in the Perales reference section at 6.12 and 6.08 Ma (e.g. Sierro et al. 2001), are not recognized.

Three influxes of *G. scitula* occurs along the section (cycles Gm12, Gm17 and Gm24). The two lowermost influxes show abundances lower than 1% (GsIa and GsIb in Fig. 5) and are not considered for biostratigraphical correlations. The more relevant influx of *G. scitula* observed in cycle Gm24 (18.4%) occurs within the acme interval of *T. multiloba* and it is therefore correlated with the second influx of *G. scitula* (event 17) observed in cycle UA29 in the Perales section, with an astronomical age of 6.099 Ma (Sierro et al. 2001).

The last occurrences (LOs) of foraminifera and calcareous nannofossils are recorded at the base and at the top of the shales of cycle Gm27 (event 19a and 19b, respectively). The tempo and mode of these events is different than in the neigbouring Pollenzo section, where the two groups, as well as foraminifera with size > 63 and < 125 μm disappear at slightly different levels (in two successive precessional cycles). In addition, in the Pollenzo section calcareous nannofossils show remarkable peaks of peculiar taxa (*Sphenolithus abies*, *Helicosphaera carteri* and *Umbilicosphaera rotula*; Lozar et al. 2018) just prior to their last occurrence that were not observed in Govone.

Based on the bioevents listed above, three planktic foraminifer subzones were identified according to Lirer et al. (2019), namely the interval Subzone MMi13c (lower part of the section, up to cycle Gm14), the interval Subzone MMi13d, from cycle Gm14 to cycle Gm27, and, finally, the Non distinctive Zone above cycle Gm27, where both foraminifera and calcareous nannofossils disappear (Fig. 6). As for the CN, the presence of *A. delicatus*, whose first occurrence (FO) best approximate the Tortonian/Messinian boundary (Hilgen et al. 2000), and of *Reticulofenestra rotaria*, a fairly reliable biostratigraphic marker in the Mediterranan region (Flores et al. 2005), clearly indicate the Messinian age of the Govone sediments. However, the distinction between the MNN11b and MNN11c zones, marked by the FO of *Nicklithus amplificus* at 6.689 Ma (Raffi et al. 2003) was not identified because of the absence of this taxon in the Govone section. The absence of *N. amplificus* is not surprising as it is generally rare and discountinously observed in other Mediterranean sections (Morigi et al. 2007). As for the magnetic intervals, the position of bioevent 12 (FAO of *T. multiloba*) in cycle Gm 12 indicates that the reversal identified at 17 m from the base of the section within cycle Gm10 can be interpreted as the C3An.2n/C3An.1r boundary, dated at 6.436 Ma (Sierro et al. 2001; Gradstein et al. 2012). Above this magnetic boundary, a thick reversal interval spans from the top of C3An.2n to the top of the sampled section; this long reversal includes bioevents 15a, 17 and 18a that in the Perales section (Sierro et al. 2001) occur within the normal C3An.1n chron. Thus, the comparison between our data and the biomagnetic pattern of the Perales section reveals that the C3An.1n chron was not recorded in the Govone section. Therefore, the base of C3r chron cannot be used to approximate the advent of the MSC, which was identified on the basis of the biostratigraphic and cyclostratigraphic patterns. The reason behind the absence of the record of C3An.1n chron probably involves the magnetic carriers and the timing of the paleomagnetic acquisition. This topic, as well as the nature of the detected ambiguous directions, needs further investigation that will be addressed in a future work.

Age model and implications for the Piedmont Basin stratigraphy

The integration of biostratigraphic, magnetostratigraphic and cyclostratigraphic data allows the bed-by-bed correlation of the Govone section with the Perales section of the Sorbas Basin (Sierro et al. 2001) and, consequently, the tuning to the 65°N summer insolation curve of Laskar et al. (2004) (Fig. 7). Although the succession of bioevents in the Govone section is consistent (homotaxic) with that recognized in Perales, some discrepancies occur in the cyclostratigraphic position of the considered bioevents. In particular, considering the C3An.2n/C3An.1r boundary as the main tie point, we observe that in Govone the LRO and LI of the *G. miotumida* gr. occur two and three precessional cycles,

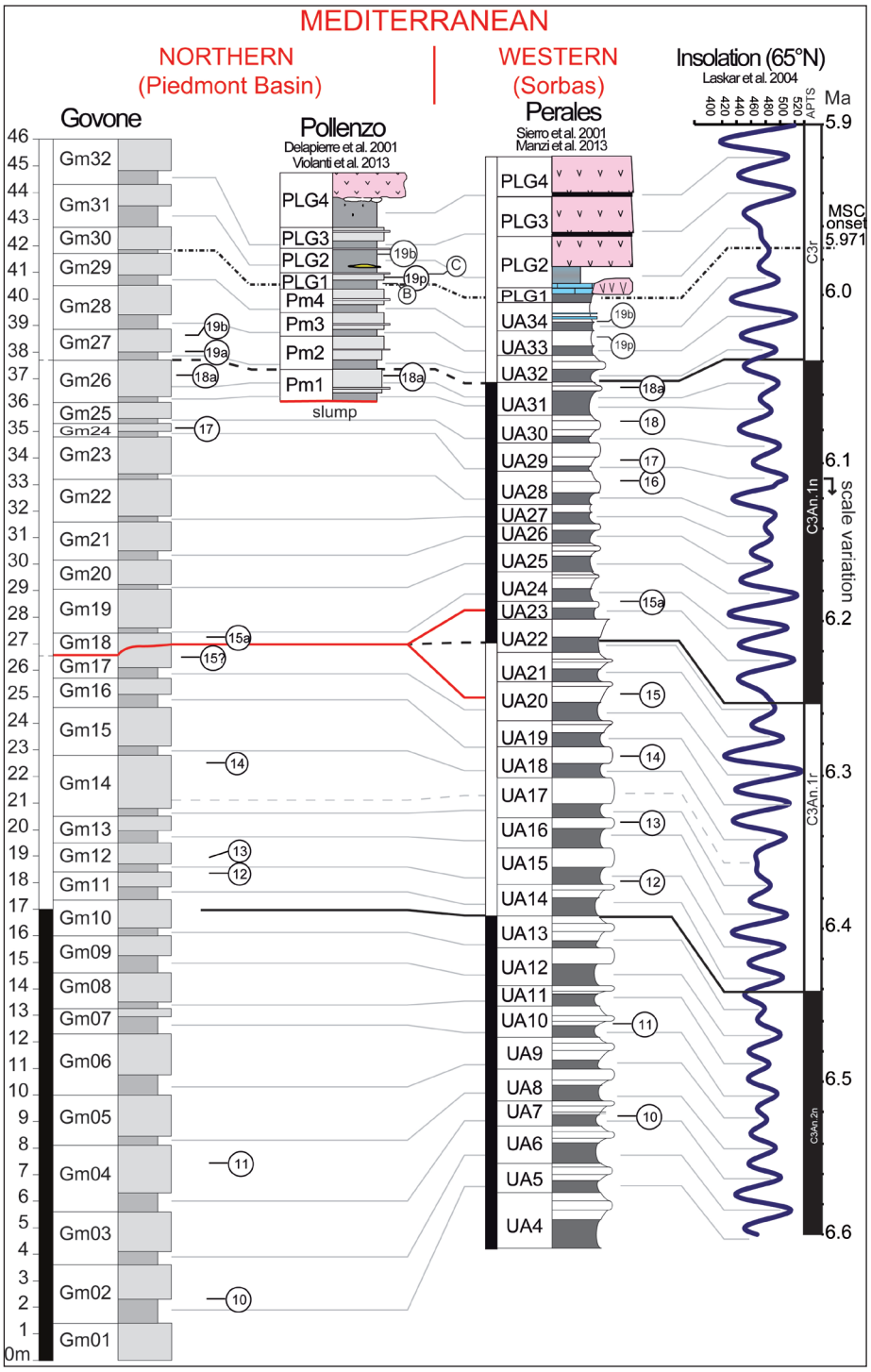

Fig. 7 - Biostratigraphic and cyclostratigraphic correlation of the Piedmont Basin sections with the Perales section of the Sorbas Basin (Sierro et la. 2001), which is tuned to the insolation curve of Laskar et al. (2004). As explained in the text, some bioevents were not detected in the Govone section and are instead present in the Perales section. These bioevents are the last abundant occurrence of the left coiled *Neogloboquadrina* gr. (13); the first influx of *G. scitula* (15); the first influx of the left coiled *Neogloboquadrina* gr. (16); the second influx of the left coiled *Neogloboquadrina* gr. (18). In both the Pollenzo and Perales section benthic foraminifera (19b) last occur sligthly after than the planktic foraminifera (19p). Among calcareous nannofossils, peaks of *Helicosphaera carteri* (B) and *Umbilicosphaera rotula* (C) were identified in the Pollenzo section close to the MSC onset. Bold correlation lines are related to magnetostratigraphy, dashed bold lines are used to interpolate the magnetic reversal in the Piedmont Basin sections where no data are available (Pollenzo) or remagnetization occurred (Govone, see text for explanation). The dash-dotted line represents the MSC onset.

respectively, in advance with respect to the Perales reference section (Fig. 7). As shown by Morigi et al. (2007), the diachroneity of these two events were already observed in the eastern Mediterranean Pissouri section. Furthermore, the highly intermittent occurrences of abundance peaks of this group and the general low abundance at the end of its range (Sierro et al. 2001) suggest that the identification of the exact position of the LRO and LI may depend on sampling resolution.

While the FAO of T. *multiloba* (cycles Gm11/12, 6.41 Ma, event 12) is consistently recorded one precessional cycle above the magnetic reversal C3An.2n/C3An.1r (6.436 Ma), the FAO of destral *N. acostaensis* (event 14) occurs in Govone at the top of the thick cycle Gm14, four cycles above the magnetic reversal instead of five as in the Perales section (Sierro et al. 2001). This early occurrence is validated by two cyclostratigraphic observations: 1) the succession of thin and thick laminated shales

in the interval comprised between cycles Gm7 and Gm14 is consistent with the pattern of the insolation curve between 6.52 and 6.4 Ma (Fig. 7). In this interval this curve is typified by less and more pronounced fluctuations of insolation maxima, originated by the precession/obliquity interference and giving rise to thinner and thicker layers of laminates shales, respectively. 2) The thickness of cycle Gm14, which suggests its correlation with the eccentricity minimum centered at 6.36 Ma (cycle UA17 in the Perales section). These observations allow to reconsider the minor influx of *G. scitula* in the cycle Gm17 (indicated as event "15?") as equivalent of the first influx documented in the Perales section (Sierro et al. 2001), three cycle above UA17 (Fig. 7). As suggested for the *G. miotumida* gr., the identification of the this *G. scitula* peak may be biased by an insufficient sampling resolution.

The erosion associated with the slump scar possibly explains the lower number of lithological cycles (10 instead of 12) between the double cycle Gm14 (i.e. the FAO of dextral *N. acostaensis*) and the straightforward second influx of *G. scitula* (Gm24, event 17) in the Govone section with respect to the Perales section (UA17-UA29). This inconsistency reflects the presence of a hiatus of two lithological cycles in correspondence of the slump scar (Fig. 7). The second influx of *G. scitula* is important to tune the upper portion of the section above the slump scar in the absence of clear sinistral influxes of the *Neogloboquadrina* gr. It allows the calibration of two additional *T. multiloba* bioevents (PE, event 15a and LO, event 18a), which were also recognized in the Perales and Tokhni sections (Gennari et al. 2018). In Govone, the PE and the LO of *T. multiloba* occur six cycles below (Gm18) and two above (Gm26), respectively, the second influx of *G. scitula* (Gm24), exactly as in the Perales section (cycles UA29 and UA31). The correlation of the LO of *T. multiloba* is strengthened by the fact that it occurs in thick double cycles (Gm26 and UA31) deposited during an eccentricity minimum. Accordingly, the onset of the MSC – corresponding to the timeline at 5.97 Ma – was indentified in the Govone section at the base of the marls of cycle Gm30, i.e. six lithological cycles above the second influx of *G. scitula* and six lithological cycles below the first gypsum bed of the PLG unit. Correlation with the Perales section indicates that the marls of cycle Gm30 correspond to the first gypsum bed of Perales (cycle PLG1, Manzi et al. 2013), which appears six cycles above the second influx of *G. scitula*. This implies that the disappearance of calcareous plankton and benthic foraminifera in the Govone section predates the MSC onset of at least three cycles compared to other Mediterranean sections, where the advent of the crisis is approximated by this bioevent (Gennari et al. 2013; Manzi et al. 2013; Violanti et al. 2013; Gennari et al. 2018 and Lozar et al. 2018). Such early disappearance is likely the result of early diagenetic processes, responsible for the dissolution of the calcareous tests, as already proposed by Dela Pierre et al. (2014) to explain the absence of calcareous tests in the lowermost gypsum-free PLG cycles of the geographically close Pollenzo section. In the pre-MSC deposits of the Govone section this hypothesis is corroborated by the decrease of calcareous nannofossil preservation and the increase in frequency of levels barren in foraminifera from cycle Gm23. However, the validation of such hypothesis requires further work, devoted to the reconstruction of the diagenetic evolution of the sediments, that is beyond the scope of this paper. Here, we stress that, unlike in Govone, in the neighbouring Pollenzo section foraminifera larger than 125 μm are recorded until the MSC onset (first PLG cycle, Fig. 7) and that small-sized foraminifera and calcareous nannofossils are still recorded above this level (Violanti et al. 2013; Lozar et al. 2018; Lozar & Negri 2019). This suggests that the disappearance of calcareous microfossils is not a synchronous event within the PB and that its position may have been controlled by a change of the preservation degree of calcareous tests.

The calibration of the LO of *T. multiloba* by means of the second influx of *G. scitula* represents an important improvement for the Messinian biochronostratigraphic framework of the Piedmont Basin. The LO of *T. multiloba* was used to build the age model of the Pollenzo section (Lozar et al. 2018 and references therein), a key section for paleoenvironmental reconstructions in the northern Mediterranean (Natalicchio et al. 2017, 2019). Outside the Piedmont Basin, this bioevent has been only used for the age model of the Tokhni section (Cyprus; Gennari et al. 2018). Remarkably, in both the Tokhni and Pollenzo sections, the LO of *T. multiloba* predates the onset of the MSC of about four precessional cycles; however, the onset of the MSC is recognized on the basis of two bioevents that still retain some uncertainty, i.e. the disappearance of foraminifera

(see above the diagenetic bias problem) and the "calcareous nannofossil bioevents" as defined in Lozar et al. (2018) and Lozar & Negri (2019). Our data indicate that the LO of *T. multiloba* is a further and easily recognizable biovent useful to approximate the onset of the MSC. A further critical aspect regarding the Govone section is the greater abundance of this taxon (ca. 30%) with respect to the Tokhni and Perales sections (<5%). However, similar contents were observed in the Pollenzo sections (Fig. 3 in Violanti et al. 2013), suggesting that the higher abundance of *T. multiloba* at the end of its range is a characteristic feature of the Piedmont Basin, not reflected in the southern Mediterranean (Sierro et al. 2001; Blanc-Valleron et al. 2002; Morigi et al. 2007).

Conclusions

The integrated study of the Govone section has provided insights in terms of both paleoenvironmental evolution and Messinian stratigraphic framework concerning the uppermost part of the pre-salinity crisis phase in the Piedmont Basin. Our dataset provide indications for lower sea surface temperature and higher nutrient content for the northern sector of the Mediterranean compared to the south-western and eastern sectors. Biomagnetostratigraphic data indicate that chron C3An.1n is not recorded in the section, pointing to the overprint of a normal polarity signal with a reverse one. Our age model also shows that calcareous microfossils disappeared before the onset of the MSC, most likely in response of diagenetic processes. In the absence of a coherent magnetostratigraphic pattern, we propose that the disappearance (LO) of *T. multiloba*, whose age is close to the top of chron C3An.1n, is the closest bioevent to the MSC onset.

Acknowledgements: This work was funded by Università di Torino funds (ex 60% 2017 and 2019) to FD. We thank Donata Violanti for her continuous support and Simona Cavagna for the preparation of micropaleontological samples. We also thank the Associate Editor G. Muttoni and two anonymous reviewers for the helpful comments and suggestions which helped to improve the manuscript.

References

Bigi G., Cosentino D., Parotto M., Sartori R. & Scandone P. (1990) - Structural model of Italy: Geodinamic Project., Consiglio Nazionale delle Ricerche (S.EL.CA, scale 1:500,000, sheet 1).

Blanc-Valleron M.M., Pierre C., Caulet J.P., Caruso A., Rouchy J.M., Cespuglio G., Sprovieri R., Pestrea S. & Di Stefano E. (2002) - Sedimentary, stable isotope and micropaleontological records of paleoceanographic change in the Messinian Tripoli Formation (Sicily, Italy). *Palaeogeography, Palaeoclimatology, Palaeoecology*, 185: 255- 286.

Bown P. R. & Young J.R. (1998) - Techniques. In: Bown P. R. (Eds) - Calcareous Nannofossil Biostratigraphy: 16-28. Kluwer Academic Publications, Dordrecht.

Catalano R., Di Stefano E., Sprovieri R., Lena G. & Valenti V. (2016) - The barren Messinian Tripoli in Sicily and its palaeoenvironmental evolution: suggestions on the exploration potential. *Petroleum Geosciences*, 22: 322-332.

Chadima M. & Hrouda F. (2006) - Remasoft 3.0 a user-friendly paleomagnetic data browser and analyzer. *Travaux Géophysiques*, 27: 20-21.

Dela Pierre F., Festa A. & Irace A. (2007) - Interaction of tectonic, sedimentary, and diapiric processes in the origin of chaotic sediments: An example from the Messinian of Torino Hill (Tertiary Piedmont Basin, northwestern Italy). *Bulletin of the Geological Society of America*, 119: 1107-1119.

Dela Pierre F., Bernardi E., Cavagna S., Clari P., Gennari R., Irace A., Lozar F., Lugli S., Manzi V., Natalicchio M., Roveri M. & Violanti D. (2011) - The record of the Messinian salinity crisis in the Tertiary Piedmont Basin (NW Italy): The Alba section revisited. *Palaeogeography, Palaeoclimatology, Palaeoecology*, 310: 238-255.

Dela Pierre F., Clari P., Bernardi E., Natalicchio M., Costa E., Cavagna S., Lozar F., Lugli S., Manzi V., Roveri M. & Violanti D. (2012) - Messinian carbonate-rich beds of the Tertiary Piedmont Basin (NW Italy): Microbially-mediated products straddling the onset of the salinity crisis. *Palaeogeography, Palaeoclimatology, Palaeoecology*, 344-345: 78-93.

Dela Pierre F., Clari P., Natalicchio M., Ferrando S., Giustetto R., Lozar F., Lugli S., Manzi V., Roveri M. & Violanti D. (2014) - Flocculent layers and bacterial mats in the mudstone interbeds of the Primary Lower Gypsum unit (Tertiary Piedmont basin, NW Italy): Archives of palaeoenvironmental changes during the Messinian salinity crisis. *Marine Geology*, 355: 71-87.

Dela Pierre F., Natalicchio M., Lozar F., Bonetto S., Carnevale G., Cavagna S., Colombero S., Sabino M. & Violanti D. (2016) - The northernmost record of the Messinian salinity crisis (Piedmont basin, Italy). *Geological Field Trips*, 8: 1-58.

Di Stefano A., Verducci M., Lirer F., Ferraro L., Iaccarino S.M., Hüsing S. & Hilgen F.J. (2010) - Paleoenvironmental conditions preceding the Messinian Salinity Crisis in the Central Mediterranean: Integrated data from the Upper Miocene Trave section (Italy). *Palaeogeography, Palaeoclimatology, Palaeoecology*, 297: 37-53.

Filippelli G.M., Sierro F.J., Flores J.A., Vázquez A., Utrilla R., Pérez-Folgado M. & Latimer J.C. (2003) - A sediment-nutrient-oxygen feedback responsible for productivity variations in Late Miocene sapropel sequences of the

western Mediterranean. *Palaeogeography, Palaeoclimatology, Palaeoecology*, 190: 335-348.

Fisher R.A. (1953) - Dispersion on a sphere. *Proceeding of the Royal Society of London*, A217: 295-305.

Flores J.-A., Sierro F.J., Filippelli G. M., Bárcena M.A., Pérez-Folgado M., Vázquez A. & Utrilla R. (2005) - Surface water dynamics and phytoplankton communities during deposition of cyclic late Messinian sapropels sequences in the western Mediterranean. *Marine Micropaleontology*, 56: 50-79.

Gennari R., Manzi V., Angeletti A., Bertini A., Biffi U., Ceregato A., Faranda C., Gliozzi E., Lugli S., Menichetti E., Rosso A., Roveri M. & Taviani M. (2013) - A shallow water record of the onset of the Messinian salinity crisis in the Adriatic foredeep (Legnagnone section, Northern Apennines). *Palaeogeography, Palaeoclimatology, Palaeoecology*, 386: 145-164.

Gennari R., Lozar F., Turco E., Dela Pierre F., Manzi V., Natalicchio M., Lugli S., Roveri M., Schreiber C. & Taviani M. (2018) - Integrated stratigraphy and paleoceanographic evolution of the pre-evaporitic phase of the Messinian salinity crisis in the Eastern Mediterranean as recorded in the Tokhni section (Cyprus island). *Newsletter on Stratigraphy*, 51: 1-23.

Ghibaudo G., Clari P. & Perello M. (1985) - Litostratigrafia, sedimentologia ed evoluzione tettonico-sedi- mentaria dei depositi miocenici del margine sud-orientale del Bacino Terziario Ligure-Piemontese (valli Borbera, Scrivia e Lemme). *Bollettino della Società Geologica Italiana*, 104: 349- 397.

Gradstein F.M., Ogg J.G., Schmitz M. & Ogg G. (2012) - The geologic time scale 2012. Elsevier, Amsterdam, 1143 pp.

Hilgen F.J. & Krijgsman W. (1999) - Cyclostratigraphy and astrochronology of the Tripoli diatomite formation (pre-evaporite Messinian, Sicily, Italy). *Terra Nova*, 11: 16-22.

Hilgen F.J., Krijgsman W., Langereis C.G., Lourens L.J., Santerelli A. & Zachariasse W.J. (1995) - Extending the astronomical (polarity) time scale into the Miocene. *Earth and Planetary Science Letters*, 136: 495-510.

Hilgen F.J., Iaccarino S., Krijgsman W., Villa G., Langereis C.G. & Zachariasse W.J. (2000) - The Global Boundary Stratotype Section and Point (GSSP) of the Messinian Stage (uppermost Miocene). *Episodes*, 23: 172-178.

Hilgen F.J., Aziz H.A., Krijgsman W., Raffi I. & Turco E. (2003) - Integrated stratigraphy and astronomical tuning of the Serravallian and lower Tortonian at Monte dei Corvi (Middle-Upper Miocene, northern Italy). *Palaeogeography, Palaeoclimatology, Palaeoecology*, 199: 229-264.

Hsü K.J., Ryan W.B.F. & Cita M.B. (1973) - Late Miocene desiccation of the Mediterranean. *Nature*, 242: 240-244.

Kaiho K. (1994) - Benthic foraminiferal dissolved-oxygen index and dissolved-oxygen levels in the modern ocean. *Geology*, 22: 719-722.

Kenig F., Sinninghe Damsté J.P., Frewin N.L., Hayes J.M., de Leeuw J.W. (1995) - Molecular indicators for palaeoenvironmental change in a Messinian evaporitic sequence (Vena del Gesso, Italy). II: high resolution variations in abundance and ^{13}C contents of free and sulphur-bound carbon skeletons in a single marl bed. *Organic Geochemistry* 23(6): 485-526.

Krijgsman W., Hilgen F.J., Raffi I., Sierro F.J. & Wilson D.S. (1999) - Chronology, causes and progression of the Messinian salinity crisis. *Nature*, 400: 652-655.

Krijgsman W., Gaboardi S., Hilgen F.J., Iaccarino S., De Kaenel E. & Laan van der E. (2004) - Revised astrochronology for the Ain el Beida section (atlantic Morocco): No glacio-eustatic control for the onset of the messinian salinity crisis. *Stratigraphy*, 1: 87-101.

Kouwenhoven T.J., Hilge, F.J. & van der Zwaan G.J. (2003) - Late Tortonian-early Messinian stepwise disruption of the Mediterranean-Atlantic connections: constraints from benthic foraminiferal and geochemical data. *Palaeogeography, Palaeoclimatology, Palaeoecology*, 198: 303-319.

Kouwenhoven T.J., Morigi C., Negri A., Giunta S., Krijgsman W. & Rouchy J.M. (2006) - Paleoenvironmental evolution of the eastern Mediterranean during the Messinian: constraints from integrated microfossil data of the Pissouri Basin (Cyprus). *Marine Micropaleontology*, 60: 17-44.

Iaccarino S., Castradori D., Cita M.B., Di Stefano E., Gaboardi S., McKenzie J.A., Spezzaferri S. & Sprovieri R. (1999) - The Miocene-Pliocene boundary and the significance of the earliest Pliocene flooding in the Mediterranean. *Memorie della Società Geologica Italiana*, 54: 109-131.

Iaccarino S.M., Bertini A., Di Stefano A., Ferraro L., Gennari R., Grossi F., Lirer F., Manzi V., Menichetti E., Ricci Lucchi M., Taviani M., Sturiale G. & Angeletti L. (2008) - The Trave section (Monte dei Corvi, Ancona, Central Italy): an integrated paleontological study of the Messinian deposits. *Stratigraphy*, 5: 283-308.

Irace A., Dela Pierre F. & Clari P. (2005) - "Normal" and "chaotic" deposits in the Messinian Gessoso-solfifera Fm. at the north-eastern border of the Langhe domain (Tertiary Piedmont basin). *Bollettino della Società Geologica Italiana, Volume speciale*, 4: 77-85.

Laskar J., Robutel P., Joutel F., Gastineau M., Correia A.C.M. & Levrard B. (2004) - A long term numerical solution for the insolation quantities of the Earth. *Astronomy and Astrophysics*, 428: 261-285.

Lirer F., Foresi L.M., Iaccarino S.M., Salvatorini G., Turco E., Cosentino C., Sierro F. & Caruso A. (2019) - Mediterranean Neogene planktonic foraminifer biozonazion and biochronology. *Earth Science Review*, 196: 102869.

Lozar F., Violanti D., Dela Pierre F., Bernardi E., Cavagna S., Clari P., Irace A., Martinetto E. & Trenkwalder S. (2010) - Calcareous nannofossils and foraminifers herald the Messinian salinity crisis: the Pollenzo section (Alba, Cuneo; NW Italy). *Geobios*, 43: 21-32.

Lozar F., Violanti D., Bernardi E., Dela Pierre F. & Natalicchio M. (2018) - Identifying the onset of the Messinian salinity crisis: A reassessment of the biochronostratigraphic tools (Piedmont Basin, NW Italy). *Newsletters on Stratigraphy*, 51: 11-31.

Lozar F. & Negri A. (2019) - A review of basin-wide calcareous nannofossil bioevents in the Mediterranean at the onset of the Messinian salinity crisis. *Marine Micropaleontology*, 151: 101752.

Lucifora S., Cifelli F., Mattei M., Sagnotti L., Cosentino D. & Roberts A.P. (2012) - Inconsistent magnetic polarities in magnetite - and greigite - bearing sediments: Understanding complex magnetizations in the late Messinian in the Adana Basin (southern Turkey). *Geochemestry, Geophysics, Geosystem*, 13: Q10002, doi:10.1029/2012GC004248.

Lugli S., Manzi V., Roveri M. & Schreiber B.C. (2010) - The Primary Lower Gypsum in the Mediterranean: a new facies interpretation for the first stage of the Messinian salinity crisis. *Palaeogeography, Palaeoclimatology, Palaeoecology*, 297: 83-99.

Manzi V., Roveri M., Gennari R., Bertini A., Biffi U., Giunta S., Iaccarino S.M., Lanci L., Lugli S., Negri A., Riva A., Rossi M.E. & Taviani M. (2007) - The deep-water counterpart of the Messinian Lower Evaporites in the Apennine foredeep: The Fanantello section (Northern Apennines, Italy). *Palaeogeography, Palaeoclimatology, Palaeoecology*, 251: 470-499.

Manzi V., Gennari R., Hilgen F., Krijgsman W., Lugli S., Roveri M. & Sierro F.J. (2013) - Age refinement of the Messinian salinity crisis onset in the Mediterranean. *Terra Nova*, 25: 315-322.

Manzi V., Gennari R., Lugli S., Persico D., Reghizzi M., Roveri M., Schreiber B.C., Calvo R., Gavrieli I. & Gvirtzman Z. (2018) - The onset of the Messinian salinity crisis in the deep Eastern Mediterranean basin. *Terra Nova*, 30(3): 189-198. https://doi.org/10.1111/ter.12325

Morigi C., Negri A., Giunta S., Kouwenhoven T., Krijgsman W., Blanc-Valleron M.M., Orszag-Sperber F. & Rouchy J.M. (2007) - Integrated quantitative biostratigraphy of the latest Tortonian-early Messinian Pissouri section (Cyprus): An evaluation of calcareous plankton bioevents. *Geobios*, 40: 267-279.

Mosca P., Polino R., Rogledi S. & Rossi M. (2010) - New data for the kinematic interpretation of the Alps-Apennines junction (Northwestern Italy). *International Journal of Earth Sciences*, 99: 833-849.

Murray J. (2006) - Ecology and Applications of Benthic. Cambridge University Press, Cambridge, 426 pp.

Natalicchio M., Birgel D., Peckmann J., Lozar F., Carnevale G., Liu X., Hinrichs K.-U. & Dela Pierre F. (2017) - An archaeal biomarker record of paleoenvironmental change across the onset of the Messinian salinity crisis in the absence of evaporites (Piedmont Basin, Italy). *Organic Geochemistry*, 113: 242-253.

Natalicchio M., Dela Pierre F., Birgel D., Brumsack H., Carnevale G., Gennari R., Gier S., Lozar F., Pellegrino L., Sabino M., Schnetge B. & Peckmann J. (2019) - Paleoenvironmental change in a precession-paced succession across the onset of the Messinian salinity crisis: Insight from element geochemistry and molecular fossils. *Palaeogeography, Palaeoclimatology, Palaeoecology*, 518: 45-61.

Perch-Nielsen K. (1985) - Cenozoic calcareous nannofossils. In: Bolli H.M., Saunders J. B. & Perch-Nielsen K. (Eds.) - Plankton Stratigraphy. Cambridge University Press, Cambridge: 427-554.

Raffi I., Mozzato C. A., Fornaciari E., Hilgen F. J. & Rio D. (2003) - Late Miocene calcareous nannofossil biostratigraphy and astrobiochronology for the Mediterranean region. *Micropaleontology*, 49: 1-26.

Rossi M. (2017) - Outcrop and seismic expression of stratigraphic patterns driven by accommodation and sediment supply turnarounds: Implications on the meaning and variability of unconformities in syn-orogenic basins. *Marine Petroleum Geology*, 87: 112-127.

Rossi M., Mosca P., Polino R. & Biffi U. (2009) - New outcrop and subsurface data in the Tertiary Piedmont Basin (NW Italy): unconformity bounded stratigraphic units and their relationships with basin modification phases. *Rivista Italiana Paleontologia e Stratigrafia*, 115: 305-335.

Roveri M., Bertini A., Cosentino D., Di Stefano A., Gennari R., Gliozzi E., Grossi F., Iaccarino S.M., Lugli S., Manzi V. & Taviani M. (2008) - A high-resolution stratigraphic framework for the latest Messinian events in the Mediterranean area. *Stratigraphy*, 5(3-4): 323-342.

Roveri M., Flecker R., Krijgsman W., Lofi J., Lugli S., Manzi V., Sierro F.J., Bertini A., Camerlenghi A., De Lange G., Govers R., Hilgen F.J., Hübscher C., Meijer P.T. & Stoica M. (2014) - The Messinian Salinity Crisis: past and future of a great challenge for marine sciences. *Marine Geology*, 352: 25-58.

Roveri M. & Manzi V. (2006) - The Messinian salinity crisis: Looking for a new paradigm? *Palaeogeography, Palaeoclimatology, Palaeoecology*, 238: 386-398.

Sabino M., Schefuβ E., Natalicchio M., Dela Pierre F., Birgel D., Bortels D., Schnetger B. & Peckmann J. (2020) - Climate and hydrologic variability in the northern Mediterranean across the onset of the Messinian salinity crisis. *Palaeogeography, Palaeoclimatology, Palaeoecology,* 545*,* doi. org/10.1016/j.palaeo.2020.109632.

Sierro F.J., Hilgen F.J., Krijgsman W. & Flores J.A. (2001) - The Abad composite (SE Spain): a Messinian reference section for the Mediterranean and the APTS. *Palaeogeography, Palaeoclimatology, Palaeoecology*, 168: 141-169.

Sierro F.J., Flores J.A., Frances G., Vazquez A., Utrilla R., Zamarreno I., Erlenkeuser H. & Barcena M.A. (2003) - Orbitally-controlled oscillations in planktic communities and cyclic changes in western Mediterranean hydrography during the Messinian. *Palaeogeography, Palaeoclimatology, Palaeoecology*, 190: 289-316.

Simon D., Marzocchi A., Flecker R., Lunt D.J., Hilgen F. J.& Meijer P.T. (2017) - Quantifying the Mediterranean freshwater budget throughout the late Miocene: new implications for sapropel formation and the Messinian salinity crisis. *Earth and Planetary Science Letters*, 472: 25-37.

Sinninghe Damsté J.S., Frewin N.L., Kenig F. & De Leeuw J.W. (1995) - Molecular indicators for palaeoenvironmental changes in a Messinian evaporitic sequence (Vena del Gesso, Italy). I: Variations in extractable organic matter of ten cyclically deposited marl beds. *Organic Geochemistry*, 23: 471-483.

Sturani C. (1973) - A fossil eel (*Anguilla* sp.) from the Messinian of Alba (Tertiary Piedmont Basin). Palaeoenvironmental and palaeogeographic implications. In: Drooger C.W. (Ed.) - Messinian Events in the Mediterranean. *Koninklijke Nederlandse Akademie van Wetenschappen*: 243-255.

Sturani C. & Sampò M. (1973) - Il Messiniano inferiore in facies diatomitica nel Bacino Terziario Piemontese. *Memorie Società Geologica Italiana*, 12: 335-338.

Vai G.B. (1997) - Cyclostratigraphic estimate of the Messinian stage duration. In: Montanari A., Odin G.S. & Coccioni R. (Eds.) - Miocene stratigraphy: an integrated approach, *Developments in Paleontology and Stratigraphy,* 15: 463-476.

Violanti D., Lozar F., Natalicchio M., Dela Pierre F., Bernardi E., Clari P. & Cavagna S. (2013) - Stress-tolerant microfossils of a Messinian succession from the Northern Mediterranean basin (Pollenzo section, Piedmont, northwestern Italy). *Bollettino della Società Paleontologica Italiana,* 52: 45-54.

Young J.R. (1999) - Neogene. In: Bown P.R. (Ed.) - Calcareous Nannofossil Biostratigraphy: 225-265. Kluwer Academic Publishers, Dordrecht.

Young J.R., Bown P.R. & Lees J.A. (2020) - Nannotax3 website. International Nannoplankton Association. Accessed 2019 through Apr. 2020. URL: http://www.mikrotax.org/Nannotax3.